

Formulation of SnO₂/graphene nanocomposite modified electrode for synergistic electrochemical detection of dopamine

R. Sriramprabha, M. Divagar, D. Mangalaraj, N. Ponpandian, C. Viswanathan*

Department of Nanoscience & Technology, Bharathiar University, Coimbatore 641 046, India

*Corresponding author. Tel: (+91) 422-2428422, Fax: (+91) 422-2422387; E-mail: viswanathan@buc.edu.in

Received: 30 May 2015, Revised: 01 August 2015 and Accepted: 08 August 2015

ABSTRACT

Pristine SnO₂ and SnO₂/Graphene (SnO₂/GN) nanocomposites were prepared via facile hydrothermal method with amended electro catalytic activity towards Dopamine (DA) sensing. X-Ray Diffraction (XRD) pattern revealed the formation of tetragonal crystal system of SnO₂ that was retained in both pure metal oxide and composite. Fourier Transform – Infrared (FT-IR) transmission spectra evidenced the stretching and bending vibration modes of pure SnO₂ and SnO₂/GN nanocomposites. The in-plane bending modes of SnO₂ and graphitic peaks in graphene oxide (GO) and composite were identified in Raman spectral analysis. Morphology of synthesized materials and uniform distribution of SnO₂ on graphene sheet in SnO₂/GN composite were observed in Field Emission-Scanning Electron Microscope (FE-SEM). Electrochemical performance of SnO₂ and SnO₂/GN nanocomposite on modified Glassy Carbon (GC) electrode was evaluated for direct DA sensing using Cyclic Voltammetry (CV), Differential Pulse Voltammetry (DPV) and Chrono Amperometric techniques. The SnO₂/GN nanocomposite showed enhanced charge carrier mobility towards DA in presence of interferences like Ascorbic acid (AA) and Uric acid (UA) compared to pristine SnO₂. The limit of detection was calculated as (0.7 μM) for (SnO₂/GN) which is better than bare SnO₂ (6.675 μM). These synergetic behaviors depicting SnO₂/GN composite can serve as a promising electrode in sensor transducers in near future. Copyright © 2015 VBRI Press.

Keywords: DA; nanocomposite; electrochemical sensor; direct electron transfer; amperometry.

Introduction

DA is an electroactive neurotransmitter which belongs to the catecholamine family. It acts as an extra synaptic messenger in brain body integration [1-4] that affects brain circuitry, neuronal plasticity, cardiovascular and also renal systems. The DA inadequacy or complete depletion causes neurological disorders like schizophrenia, Parkinson's disease, and ADHD/ADD. Owing to their greater physiological and pathological significances, accurate and selective measurements of DA at low detection limits in living system are of great interest [5-6]. Since last few eras, there are several analytical methods have been developed for the detection of DA [7] engaging with complex detection approaches, electrochemical methods follow simple and sensitive strategies [8] in evaluating the low concentration of DA under physiological conditions.

Striking efficiency of the sensor depends mainly on the selection of materials for fabricating the electrodes and choosing the electrolytes with desirable qualities. Semiconductor metal oxides (MOx) nanostructures are owning unique and refined functional properties due to their crystallographic structures, morphology and dimension compared to their bulk form. Among them SnO₂

is one of the promising candidate having wide band gap and catalytic properties hence played remarkable role in variety of sensor applications [9]. Their technological importance in catalytic process makes them to serve as working electrodes predominantly in variety of sensor applications [10, 11]. Though the oxide surface having great efficacy in determining binding affinity with adsorbates and charge transport between analyte and electrode, it indeed to be enhanced by surface modifications to promote their sensitivity and selectivity.

Graphene is one of the most anticipate carbon structure known for its high charge carrier mobility, transparent, self-standing properties like large surface area and better chemical, thermal and electrical stabilities [12-16]. When graphene incorporated with MOx nanoparticles, it acting as a supporting matrix and facilitate the MOx with active redox sites for further tuning its intrinsic properties. There have been many research works are focused on metal oxide Graphene-MOx nanocomposite like Graphene/CuO, Graphene/TiO₂, Graphene/Fe₃O₄ and Graphene/SnO₂ for high detection in bio and chemical sensors [17-20]. There are several physical and chemical methods are in practice to prepare the Graphene-MOx nano structures, among them

chemical methods are preferred because of their simplicity, less expensive and time consuming abilities. Even though metal oxide–graphene nanocomposites prepared by using selective chemical method with desirable qualities for sensor applications only few reports are available in selective and simultaneous detection of DA among the interference molecules like AA and UA due to their redox potential which lies closer to DA.

In our present study, we prepared SnO₂ and SnO₂/GN nanocomposites by a facile and cost effective hydrothermal method. We carefully adjusted the physical and chemical reaction parameters there by retained the constancy in crystal structure of metal oxide in nanocomposites with bare metal oxide [21]. The crystal structure is one of the most ambitious factors that directly influence the physico-chemical properties of materials. We synthesized pristine metal oxide and Graphene nanocomposites in pure form and they were used as electrodes for the electrochemical detection of DA. Many researchers have greatly contributed for the sensitive detection of DA using MOx and carbon based electrodes, only few reports are available on the performance of MOx-Graphene hybrid material in DA detection. This fact motivated us to study the electrocatalytic behavior of synthesized metal oxide and composite materials and sensibly compare their efficiency in DA detection. We proposed simple and effective electrochemical detection of DA with enhanced selectivity and sensitivity in presence of AA and UA as interferences.

Experimental

Material

Natural Graphite flakes, Stannous chloride pentahydrate (98%, SnCl₄·5H₂O), DA were purchased from Sigma Aldrich, NaOH, H₂O₂, KMnO₄, NaNO₃, H₂SO₄, Na₂HPO₄, NaH₂PO₄ and ethanol were of analytical grade and used without further purification. Double distilled water (DD water) was used throughout the experiments.

Synthesis of SnO₂ and SnO₂/GN nanocomposite

The starting precursor stannous chloride pentahydrate SnCl₄·5H₂O (0.1 M) was dissolved in 40ml of DD water with constant stirring and NaOH (0.2 M) was added drop wise in to the above mixture until the pH 9 was reached. The above solution was kept at Teflon Autoclave at 180 °C for 4 hrs and the resultant product was washed several times with water and ethanol simultaneously to remove the unreacted species and kept for calcinations at 800 °C for 4 hrs which provided pristine SnO₂ nanoparticles.

Graphene oxide (GO) was prepared by modified Hummers method [20]. The SnO₂/GN nanocomposite was synthesized by adding SnCl₄·5H₂O (0.1 M) in 40 ml of uniformly dispersed GO solution (1 mg/ ml) and NaOH was added to adjust the pH up to 9. The prepared mixture was kept in sealed Autoclave at 180 °C for 4hrs which yielded a composite black in colour. The product was further washed by centrifugation in ethanol and water several times at 7000 rpm for maximum purification. The end product was calcined at 250 °C for 12 hrs.

Characterization of synthesized materials

The structural, morphological and electrochemical properties of GO, SnO₂ and SnO₂/GN nanocomposite were analyzed by following techniques. The crystal structure of developed materials were characterized by Rigakumini flex II X-ray diffractometer with Cu-Kα as source radiation (λ= 1.5406 Å). The functional groups of prepared materials were confirmed using Fourier transform infrared (FT-IR) spectra recorded on a Bruker Tensor 27 FT-IR spectrophotometer. The different vibration modes of SnO₂ and nanocomposite were studied using Raman spectrometer (Horiba Jobin vyon) with Ar⁺ (λ=514 nm) laser. The morphological analyses were done by using FESEM-Quanta-250-FEG) at the acceleration potential of 30 kV.

The electrochemical analyses were carried out by Bio-Logic SP-50 electro chemical workstation. The three electrode cell was constructed using Pt wire as a counter electrode, Ag-AgCl as reference electrode and SnO₂ and SnO₂/GN on GC modified electrode as working electrodes respectively. The electrocatalytic behavior towards DA detection accompanied with other interference analytes has been measured.

Results and discussion

Morphological analyses

FE-SEM results demonstrated randomly oriented sheet like structure of GO that can be clearly seen in **Fig. 1(a)** with lower and higher magnifications. The sphere like nature of SnO₂ is observed **Fig. 1(b)** and its average size was estimated as 20 nm. While examined the morphology of nanocomposite (SnO₂/GN), the graphene sheets are obvious in lower magnification and the SnO₂ nanoparticles were distributed sporadically on graphene sheet which is evidenced in **Fig. 1(c)** at higher magnification.

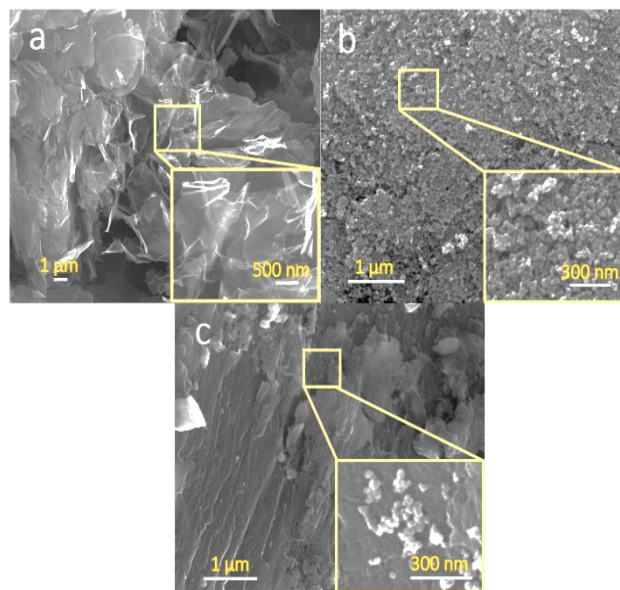


Fig. 1. FE-SEM image of (a) GO, (b) SnO₂ and (c) SnO₂/GN nanocomposite.

Structural analyses

Fig. 2(a) shows the XRD pattern of synthesized SnO₂, GO and SnO₂/GN nanocomposites. The prominent peak at [2θ=11.3°] and broadened peak at (19-28°) confirmed the presence of GO. The peaks obtained for both metal oxide and composite revealed tetragonal crystal system of SnO₂ with prominent peaks which well agreed with the literature pattern (JCPDS # 02-1340). The average grain size of the SnO₂ nanoparticles was calculated as 14 nm using Scherer's formula. The tetragonal structure of SnO₂ retained along with the graphitic peak (G* at 2θ = 22°) in XRD spectra of composite proved that the crystal structure has not been affected by the formation of composite [22, 23]. Generally attempts to improve electronic and mechanical stability of materials by the addition of other supporting matrices may alter the structure of parent material and bring down the efficiency in other aspects. However in our case, our aim to retain the crystal structure was attained with the aid of suitable synthesis materials and method.

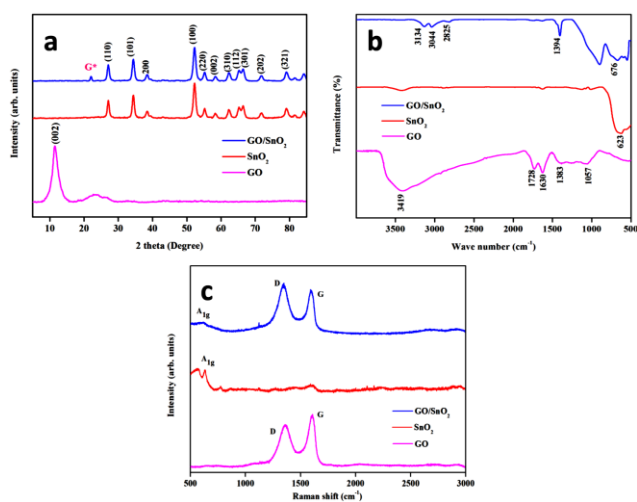


Fig. 2. (a) XRD pattern of GO, SnO₂ and SnO₂/GN, (b) FT-IR spectra of GO, SnO₂ and SnO₂/GN and (c) Raman spectra of GO, SnO₂ and SnO₂/GN nanocomposite.

Functional and elemental analyses

Fig. 2(b) displays the FT-IR spectra of the synthesized GO, SnO₂ and SnO₂-GN nanocomposites. A broad peak appeared in GO spectrum depicted the presence of O-H and C-H stretching. A prominent peak at 623 cm⁻¹ in the SnO₂ spectrum revealed the presence of the vibration mode of O-Sn-O without any impurities in pristine SnO₂. Sn-OH vibration modes in SnO₂/GN nanocomposite were found in the range 549-676 cm⁻¹. The spectra also portrayed the C=C (Sp²-hybridization) peak at 1638 cm⁻¹ and another significant peak at 1728 cm⁻¹ corresponding to weak O-H bending mode. Reduction of graphene oxide to graphene in the composite can be confirmed from the separated peaks (2825-3134 cm⁻¹) which appeared broadened in GO spectrum. Peak at 893 cm⁻¹ referred (O-C=O) vibration mode in aromatic carbon. The inclusion of Sn⁴⁺ ions into the graphene sheets almost decimated the oxygen containing groups at 1394 cm⁻¹ (C-O and C-OH deformation) [20] in composites which explicitly present in

GO spectrum (1400-1057 cm⁻¹) used to confirm the reduction of GO into graphene in SnO₂/GN composite. Further the three peaks at 2800-3200 cm⁻¹ corresponding to C-H stretching and bending vibrations.

The significant structural changes occurring during the chemical processing from SnO₂ to SnO₂/GN are reflected in their Raman spectra which are shown in **Fig. 2(c)**. The two peaks observed at 617 and 491 cm⁻¹ corresponds to the A_{1g} and E_g vibrational modes of SnO₂ nanoparticles. The band at about 567 cm⁻¹ corresponds to the in-plane oxygen vacancy at the SnO₂ nanocrystalline surface. The Raman spectrum of GO contains G band at 1580 cm⁻¹ evidenced the sp² hybridization and D band at 1350 cm⁻¹ referred the zero order boundary phonon. The D/G ratio of SnO₂/GN composites count greater in Raman spectra implies the sp² domain size is decreased upon reduction of GO in exfoliated graphene nanosheets. The characteristic peak of SnO₂ was in range of 625-632 cm⁻¹ it evidenced the existence of SnO₂ in SnO₂/GN composite which is consistent with the earlier results [24].

Electrochemical analysis of SnO₂ and SnO₂/GN nanocomposite

CV analysis of SnO₂/GCE and SnO₂/GN/GCE: The electrochemical performances of SnO₂/GCE and SnO₂/GN/GCE modified electrodes were evaluated in Phosphate Buffer Solution (PBS) with different pH (4, 5, 6, 7, 7.4 & 8) at the scan rate of 50 mV/s and 1 mM DA concentration. Similarly, the impact of distinct scan rates and concentrations of analyte on the electrochemical behavior at optimal pH have also been studied.

Fig. 3 (a) and (b) depicts the effect of pH at different values (pH = 4, 5, 6, 7, 7.4 & 8) with the variations in redox potential of DA and the differences in amount of current density. Whereas moved from neutral to more acidic pH, there was poor reversible redox reaction was observed due to lacking of the activation energy required to oxidize the positively charged DA in SnO₂/GCE. In the case of composite material, high charge mobility on graphene sheet might provide redox site for DA which can be clearly observed in **Fig. 3(b)**. The increment in oxidation current density and negative shift observed in redox potential at pH = 6 indicated the higher electron transfer in DA oxidation [25, 26]. While increasing the pH beyond 6 to 8 resulting gradual step down in reversibility and also influenced further potential shift in negative scale which is due to quasi reversible reaction [27]. Finally the optimal pH = 6 was confirmed from results and used for further electrochemical analyses.

The scan rate also possessed notable impact in the rate and kinetics of electrochemical reaction, which is shown in **Fig. 3(c) and (d)**. When scan rate was varied in the range 20- 500 mV/s there was a corresponding change observed in the current density. The steady increment in the current density along with the scan rate agreed well with the earlier result [10].

An ability of a sensor is mainly determined with its response to the analyte concentration. In the present study, the concentration of DA was varied from 0 to 10 mM in the PBS with pH 6 at the scan rate 50 mV/s to observe the

changes in redox current density and potential. It is obvious from the **Fig. 3(e)** and **(f)** corresponding to SnO_2 and composite that there is linear increase in the current density when the concentration of the DA is increased. This is due to the charge interactions between the analyte and electrode materials.

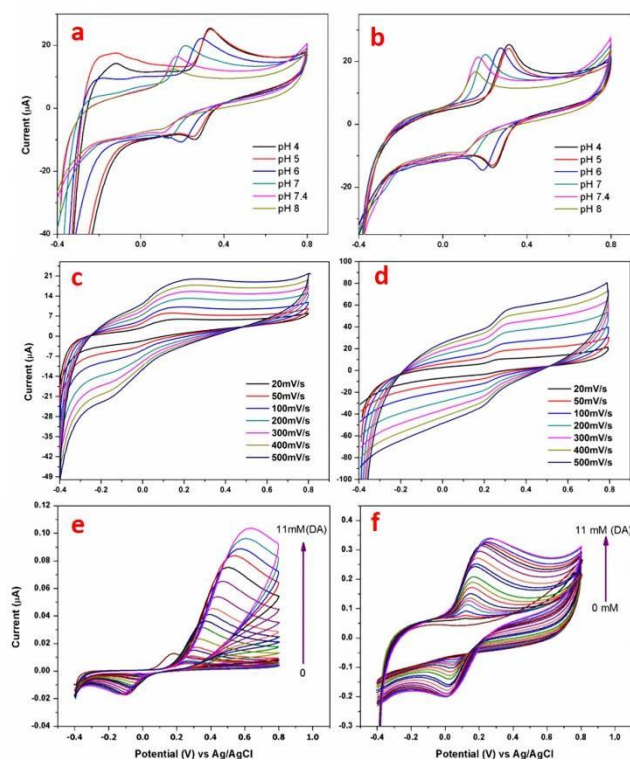


Fig. 3. Cyclic Voltammetric analysis of SnO_2/GCE (a) at different pH values (c) at different scan rates (e) at different concentrations and $\text{SnO}_2/\text{GN}/\text{GCE}$ (b) at different pH values (d) at different scan rates and (f) at different concentrations.

DPV analysis of SnO_2/GCE and $\text{SnO}_2/\text{GN}/\text{GCE}$: DPV analysis is preferred for selective and sensitive determination of analytes. The parameters used in electrochemical analyses like potential range (-0.2 V to 0.6 V), pulse amplitude (50 mV), pulse width (0.02 s) and scan rate (8 mV/s) were fixed initially. The DPV analysis was carried out for the detection of single analyte by varying its concentration keeping the other two analyte concentration as fixed. **Fig. 4(a)** shows the DPV response varying Uric acid concentration (50 to 500 μM) in presence of constant DA concentration (5 μM) but there is no significant response obtained for AA on SnO_2/GCE . In **Fig. 4(b)** we can see the individual responses for AA, DA and UA in $\text{SnO}_2/\text{GN}/\text{GCE}$ and linear variation in oxidation current over the UA concentration (50 to 500 μM) respectively. In **Fig. 4(c)** and **(d)** the DPV peak current was proportional to DA concentration over a range of 10 μM to 300 μM and 1 μM to 150 μM on SnO_2/GCE and $\text{SnO}_2/\text{GN}/\text{GCE}$ respectively. The presence of AA and UA has negligible influence on selective determination of DA. **Fig. 4(e)** shows the comparative DPV analysis on SnO_2 and $\text{SnO}_2/\text{GN}/\text{GCE}$ nanocomposite electrodes towards the detection of DA in presence of interferences. It is obvious from the result that $\text{SnO}_2/\text{GN}/\text{GCE}$ displayed individual

and accurate response for lower concentration of DA in presence of multifold volume of AA and UA at their respective potential values whereas SnO_2/GCE failed to give response to AA [28-30].

Amperometric analysis: **Fig. 4(a)** and **(b)** shows the amperometric studies of SnO_2/GCE and $\text{SnO}_2/\text{GN}/\text{GCE}$ by applying the potential of 0.5 V for the detection of DA with different concentration from 0.1 μM to 500 μM . While increasing the concentration of DA the amperometric current response was also increased. The analyte concentration was varied for every 60 Sec and the analyte was added consecutively thrice to check the repeatability. SnO_2 showed notable catalytic response to higher concentration of an analyte whereas composite exposed even for trace level.

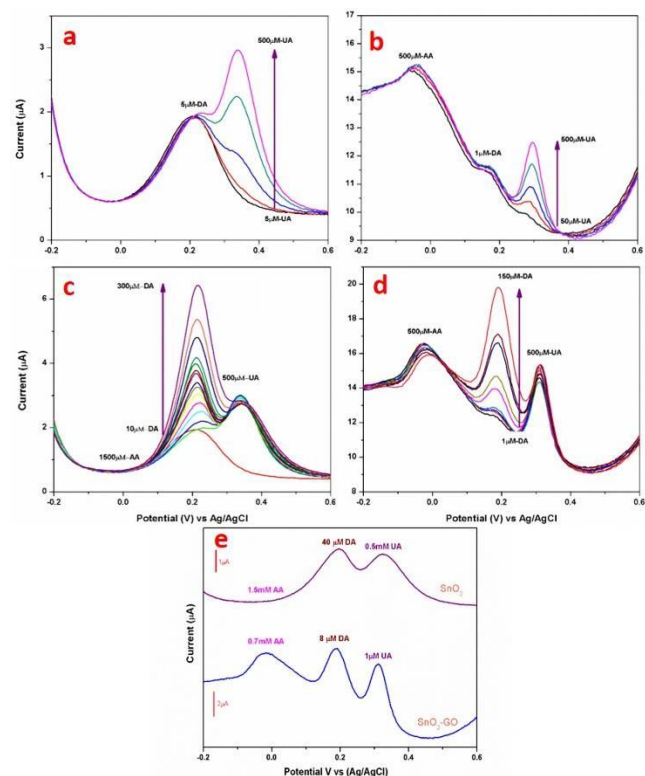


Fig. 4. Differential Pulse Voltammetry of SnO_2/GCE and $\text{SnO}_2/\text{GN}/\text{GCE}$ [(a) and (b)], at constant concentration of uric acid [(c) and (d)] at constant concentration of DA, (e) Comparative analysis of DA in presence of AA & UA on SnO_2/GCE and $\text{SnO}_2/\text{GN}/\text{GCE}$.

We examined the linear range in analyte detection as 10 – 60 μM for SnO_2 and 0.3 – 18.8 μM for SnO_2/GN which demonstrated the composite response was better in analyte detection even in nano mole concentration. The limit of detection (LOD) was calculated for SnO_2 and SnO_2/GN that are 6.675 μM and 0.717 μM respectively. From the results composite showed better electro catalytic behavior than the pristine SnO_2 . This is because of composite with enhanced carrier mobility which provided active redox site to the analyte even in trace level among the large volume of interference which is also evident from CV and DPV analysis.

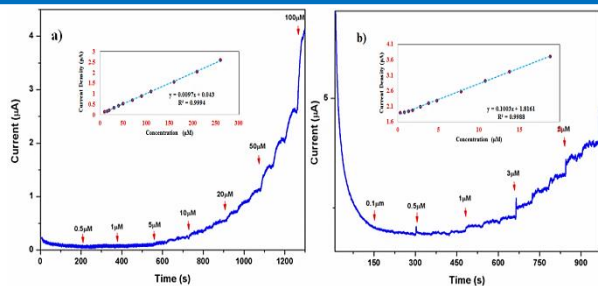


Fig. 5. Amperometric analysis of a) SnO₂/GCE and b) SnO₂/GN/GCE.

Conclusion

We prepared SnO₂ and SnO₂/Graphene nanocomposite by a simple cost effective hydrothermal method. The physico-chemical characterizations were used to confirm the structural and morphological characteristics of synthesized SnO₂ and nanocomposite materials. The electro catalytic behavior of pristine SnO₂ and SnO₂/GN composite towards detection of DA have been studied using CV, DPV and Amperometric techniques. The CV results are evidenced that coexistence of graphene in composite with SnO₂ provided a platform for the improved charge transfer there by enhanced the selectivity and sensitivity compared to bare SnO₂. The DPV and amperometric outcomes confirmed that the DA sensing was accurate in the presence of large volume of AA and UA as interference compounds even in lower concentration of DA and the Chrono amperometric test result evidenced the great linearity with LOD in nano mole of DA concentration. Thus, the SnO₂/GN nanocomposite with amended properties will pave the way for developing simple and synergetic electrode for non-enzymatic sensor platforms that can be used in real time applications.

Acknowledgements

This work was supported by Department of Science and Technology - Science and Engineering Research Board (DST-SERB), Govt of India [SR/FTP/PS-153/2011]. One of the authors C. Viswanathan gratefully acknowledge DST-SERB for awarding FAST TRACK SCHEME FOR YOUNG SCIENTIST. The authors sincerely admit their thanks to DST-PURSE for providing FE-SEM facility.

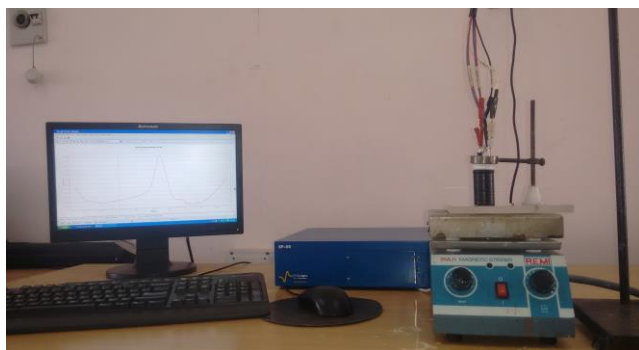
Reference

- Mahavir P Tiwari.; Rashmi M.; Deepak K.; Darshika J.; Bhim B Prasad.; *Adv. Mat. Lett.*, **2011**, 2,4, 276.
DOI: [10.5185/amlett.indias.202](https://doi.org/10.5185/amlett.indias.202)
- Wightman RM.; May LJ.; Michael AC.; *Anal Chem.*, **1988**, 60, 769A.
DOI: [10.1021/ac00164a718](https://doi.org/10.1021/ac00164a718)
- Girault JA.; Greengard P.; *Arch. Neurol.*, **2004**, 61, 5, 641.
DOI: [10.1001/archneur.61.5.641](https://doi.org/10.1001/archneur.61.5.641)
- P. Manivel.; M. Dhakshnamoorthy.; A. Balamurugan.; N. Ponpandian.; D. Mangalaraj.; C. Viswanathan.; *RSC Adv.*, **2013**, 3, 14428.
DOI: [10.1039/C3RA42322K](https://doi.org/10.1039/C3RA42322K)
- Xu, X.; Lin, Q.; Liu, A.; Chen, W.; Weng, X.; Wang, C.; Lin, X.; *Chem. Pharm. Bull.*, **2010**, 58, 788.
DOI: [10.1248/cpb.58.788](https://doi.org/10.1248/cpb.58.788)
- Krystyna Jackowska.; Pawel Kryszinski.; *Anal Bioanal Chem.*, **2013**, 405, 3753.
DOI: [10.1007/s00216-012-6578-2](https://doi.org/10.1007/s00216-012-6578-2)
- Xu X.; Zhang H.; Shi H.; Ma C.; Cong B.; Kang W.; *Anal Biochem.*, **2012**, 427, 1, 10.
DOI: [10.1016/j.ab.2012.04.022](https://doi.org/10.1016/j.ab.2012.04.022)
- Liu Y.; Huang J.; Hou H.; You T.; *Electrochem. Commun.*, **2008**, 10, 1434.

- DOI: [10.1016/j.elecom.2008.07.020](https://doi.org/10.1016/j.elecom.2008.07.020)
- Ingo P.; Viktor H.; Sören K.; Vasili C.; Oleg L.; Tudor B.; Viola D.; Ion T.; Lorenz K.; Rainer A.; Yogendra Kumar M.; *Adv. Electron. Mater.*, **2015**, 1500081.
DOI: [10.1002/aeml.201200081](https://doi.org/10.1002/aeml.201200081)
- Sivakumar Palanisamy.; *Electrochimica Acta.*, **2014**, 138, 302.
DOI: [10.1016/j.electacta.2014.06.131](https://doi.org/10.1016/j.electacta.2014.06.131)
- Tashkhourian J.; Nezhad M., R., H.; Khodavesi, J.; Javadi, S.; *J. Electroanal. Chem.* **2009**, 633, 85.
DOI: [10.1016/j.jelechem.2009.04.028](https://doi.org/10.1016/j.jelechem.2009.04.028)
- Youxing Fang.; Erkang Wan.; *Chem. Commun.*, **2013**, 49, 9526.
DOI: [10.1039/c3cc44735a](https://doi.org/10.1039/c3cc44735a)
- Nanda Gopal Sahoo.; Yongzheng Pan.; Lin Li.; Siew Hwa Chan.; *Adv. Mater.*, **2012**, 24, 4203.
DOI: [10.1002/adma.201104971](https://doi.org/10.1002/adma.201104971)
- Giovanni Neri.; Salvatore Gianluca Leonardi.; Mariangela Latino.; Nicola Donatoc.; Seunghwan Baek.; Donato E. Contee.; Patrícia A. Russoe.; Nicola Pinna.; *Sens. Actuators B.*, **2013**, 179, 61.
DOI: [10.1016/j.snb.2012.10.031](https://doi.org/10.1016/j.snb.2012.10.031)
- Matthias M.; Armim S.; Yogendra Kumar M.; Sören K.; Rainer A.; Andriy L.; Lorenz K.; Karl S.; *Adv. Mater.* **2012**, 24, 3490.
DOI: [10.1002/adma.201200491](https://doi.org/10.1002/adma.201200491)
- Ying W.; Yueming L.; Longhua T.; Jin L.; Jinghong L.; *Electrochem. Commun.* **2009**, 11, 892.
DOI: [10.1016/j.elecom.2009.02.013](https://doi.org/10.1016/j.elecom.2009.02.013)
- F. Chen.; Q. Qing.; J. Xia.; N. Tao.; *Chem. Asian J.*, **2010**, 5, 2144.
DOI: [10.1002/asia.201000252](https://doi.org/10.1002/asia.201000252)
- Giovanni Neria.; Salvatore Gianluca Leonardi.; Mariangela Latinob.; Nicola Donatoc.; Seunghwan Baekd.; Donato E. Contee.; Patrícia A. Russoe.; Nicola Pinnad.; *Sens. Actuators*, **2013**, B 179, 61.
DOI: [10.1016/j.snb.2012.10.031](https://doi.org/10.1016/j.snb.2012.10.031)
- Mingxi C.; Congcong Z.; Lingzhi L.; Yu L.; Xichuan L.; Xiaoyang X.; Fengling X.; Wei W.; Jianping G.; *ACS Appl. Mater. Interfaces*, **2013**, 5, 13339.
DOI: [10.1021/am.404195u](https://doi.org/10.1021/am.404195u)
- Teo Peik-See.; Alagarsamy Pandikumar.; Huang Nay-Ming.; Lim Hong-Ngee.; Yusran Sulaiman.; *Sensors*, **2014**, 14, 15227.
DOI: [10.3390/s140815227](https://doi.org/10.3390/s140815227)
- Chao Zhong.; Jiazhao Wang.; Zhixin Chen.; Huakun Liu.; *J. Phys. Chem. C.*, **2011**, 115, 25115.
DOI: [10.1021/jp2061128](https://doi.org/10.1021/jp2061128)
- Sungjin Park.; Jinho An.; Jeffrey R. Potts.; Aruna Velamakanni.; Shanthy Murali.; Rodney S. Ruoff.; *Carbon*, **2011**, 49, 3019.
DOI: [10.1016/j.carbon.2011.02.071](https://doi.org/10.1016/j.carbon.2011.02.071)
- Marappan Sathish.; Satoshi Mitani.; Takaaki Tomai.; Atsushi Unemoto.; Itaru Honma.; *J Solid State Electrochem.*, **2012**, 16, 1767.
DOI: [10.1007/s10008-012-1669-8](https://doi.org/10.1007/s10008-012-1669-8)
- Yueming Li.; Xiaojun Lv.; Jin Lu.; Jinghong L.; *J. Phys. Chem. C.*, **2010**, 114, 21770.
DOI: [10.1021/jp1050047](https://doi.org/10.1021/jp1050047)
- Elahé Molaakbaria.; Ali Mostafavia.; Hadi Beitollahi.; *Sens. Actuators B.* **2015**, 208, 195.
DOI: [10.1016/j.snb.2014.10.130](https://doi.org/10.1016/j.snb.2014.10.130)
- Stela Pruneanu.; Alexandru R. Biris.; Florina Pogacean.; Crina Socaci.; Maria Coros.; Marcela Corina Rosua.; Fumiya Watanabe.; Alexandru S. Biris.; *Electrochimica Acta*, **2015**, 154, 197.
DOI: [10.1016/j.electacta.2014.12.046](https://doi.org/10.1016/j.electacta.2014.12.046)
- Su-Juan Li.; Jun-Zhi He.; Meng-Jie Zhang.; Rong-Xia Zhang.; Xia-Lei Lv.; Shao-Hua Li.; Huan Pang.; *Electrochimica Acta*, **2013**, 102, 58.
DOI: [10.1016/j.electacta.2013.03.176](https://doi.org/10.1016/j.electacta.2013.03.176)
- Huiwen Wang.; Fangfang Ren.; Ruirui Yue.; Caiqin Wang.; Chunyang Zhai.; Yukou Du.; *Colloids and Surfaces A: Physicochem. Eng. Aspects.*, **2014**, 448, 181.
DOI: [10.1016/j.colsurfa.2014.02.028](https://doi.org/10.1016/j.colsurfa.2014.02.028)
- Alagarsamy Pandikumar.; Gregory Thien Soon How.; Teo Peik See.; Fatin Saiha Omar.; Subramaniam Jayabal.; Khosro Zangeneh Kamali.; Norazriena Yusoff.; Asilah Jamil.; Ramasamy Ramaraj.; Swamidoss Abraham John.; Hong Ngee Lim.; Nay Ming Huang.; *RSC Adv.*, **2014**, 4, 63296.
DOI: [10.1039/c4ra13777a](https://doi.org/10.1039/c4ra13777a)
- Jingjing Jiang.; Xuezhong Du.; *Nanoscale*, **2014**, 6, 11303.
DOI: [10.1039/c4nr01774a](https://doi.org/10.1039/c4nr01774a)

Supporting information

1. Electrochemical experimental Setup



2. Limit of Detection (LOD) calculation :

Based on the standard deviation of responses and the slope.

Regression linear based $LOD = 3.3 (SD / S)$,

LOD - Limit of Detection (in Mole)

SD - Standard deviation of the response

S - Slope